Journal of Alloys and Compounds 504 (2010) L46–L50

Contents lists available at ScienceDirect

Journal of Alloys and Compounds

journal homepage: www.elsevier.com/locate/jallcom

Letter

Controlled synthesis of Fe_3O_4 nanosheets via one-step pyrolysis of EDTA ferric sodium salt

Lingyun Chen*, Chenglan Zhao, Yang Zhou, Hui Peng, Yiyang Zheng

College of Chemistry and Chemical Engineering, Chongqing University, Chongqing 400030, PR China

ARTICLE INFO

Article history:
Received 7 April 2010
Received in revised form 22 May 2010
Accepted 29 May 2010
Available online 11 June 2010

Keywords:
Fe_3O_4 nanosheet
EDTA ferric sodium salt
Pyrolysis
Magnetic property
Magnetic materials

ABSTRACT

We present a facile one-step approach to large-scale production of single-crystal magnetite Fe_3O_4 nanosheets (NSs) employing a solid-state thermal decomposition route without the assistance of any template, carrier gas, and other additions. Single-crystal Fe_3O_4 NSs with average edge length in the range of 80–100 nm and thickness of about 30 nm were synthesized on a large scale via direct pyrolysis of inorganic–organic hybrid EDTA ferric sodium salt in a one-end closed and horizontal quartz tube furnace in the air. A series of techniques, including XRD, IR, TEM, HRTEM, and TGA, were used to characterize the final products. The HRTEM image obtained from a typical individual nanosheet displays a highly symmetrical lattice, which reveals the single-crystalline nature of the obtained Fe_3O_4 NSs. Furthermore, a possible formation mechanism from EDTA ferric sodium salt to Fe_3O_4 was also discussed. All the obtained Fe_3O_4 NSs are ferromagnetic at room temperature. This method is simple and facile and could synthesize other metal oxides under such experimental conditions.

1. Introduction

Over the past decade, magnetite (Fe_3O_4) has been widely studied due to its unique structure and novel optical, electronic, magnetic, and catalytic properties. Fe_3O_4 nanostructures, in particular, have attracted intensive attention owing to their numerous applications in information storage, ferro-fluids, magnetic refrigeration, catalysis, bio-medicine, etc. [1–8]. For these reasons, a variety of zero-dimensional (0D), 1D, 2D, and 3D Fe_3O_4 nanostructures with shapes of particles, spheres, polyhedra, belts, tubes, plates, and flowers have been successfully synthesized by many methods such as coprecipitation, micro-emulsion, hydrothermal, and microwave-assisted synthesis so far. For instance, Fe_3O_4 nanoparticles with sizes altering from 15 to 190 nm have been synthesized by solvothermal decomposition of $FeCl_3$ using mixed surfactants of sodium lauryl sulfate (SDS) and polyethylene glycol (PEG) as protective reagents [9]. Fe_3O_4 nanospheres were prepared at 180 °C via a hydrothermal reduction route in the presence of $FeCl_3$, template polyethylene glycol 4000 and the complex reagent NaAc [10]. Fe_3O_4 hierarchically hollow nanospheres organized by nanosheets of a layer-structured ferrous precursor were synthesized by a microwave-assisted hydrothermal method using ferric chloride ($FeCl_3$) as the iron source and ethylene glycol (EG) as both a solvent and a reductant in the presence of sodium hydroxide (NaOH) and sodium dodecyl benzene sulfonate (SDBS) [11]. Fe_3O_4 nanobelts have been synthesized using a facile and efficient approach by hydrothermal treatment of $FeCl_2$ and PEG-6000 at 180 °C for 17 h. [12]. Fe_3O_4 nanorings, self-assembled by nanocubes of Fe_3O_4, have been synthesized by strong magnetic dipolar attractions [13]. Fe_3O_4 nanoplates were synthesized using a simple template-free solvothermal treatment of $FeCl_3{\cdot}6H_2O$, diglycol, and NaAc at 200 °C. [14]. Fe_3O_4 nanoflowers were produced by thermal decomposition of the mixture of $Fe(acac)_3$ (acac = acetylacetonate), poly(ethylene glycol) bis(carboxymethyl) ether, oleylamine and phenyl ether in solution [15]. However, all of the reported Fe_3O_4 nanostructures were synthesized based on performed templates or thermal hydrolysis of iron salts in the presence of surfactants and the use of toxic reagents, such as organoamine and hydrazine hydrate, which have low yield and require explicated or extricated conditions. Therefore, it remains a great challenge to develop simple methods in terms of low-cost and facile synthesis before they can be useful for commercial applications.

From the crystallographic viewpoint and growth mechanism, solid-state thermal decomposition method has been regarded as one of reasonable and in situ approaches due to its simple and facile processing, short reaction time, and homogeneous products [16–19]. However, conventional solid-state thermal decomposition synthesis of metal oxide nanostructures faces two difficulties: inhibiting particulate agglomeration and promoting phase formation [20,21]. In previous work, controlling the physical properties of metal oxides, such as dispersity, composition, grain size, crystallite morphology, crystalline phase, and specific surface area, was usually performed by choosing ideal precursors. Moreover, in terms of preventing resultant particles from agglomerating

* Corresponding author. Tel.: +86 23 65673443.
E-mail address: lychen@cqu.edu.cn (L. Chen).

0925-8388/$ – see front matter © 2010 Elsevier B.V. All rights reserved.
doi:10.1016/j.jallcom.2010.05.165

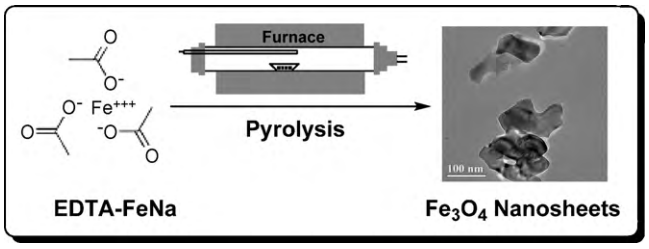

Scheme 1. Schematic illustration of the synthesis of Fe_3O_4 NSs from EDTA–FeNa.

and sintering, the desirable results have never been achieved. In many cases, nanostructures rather than nanosized products were obtained through a solid-state thermal decomposition synthesis [22–24]. Therefore, it is still a challenge to controlling the size and morphology of metal oxide nanostructures during the solid-state thermal decomposition process. We have focused on the construction of novel nano- and micromaterials such as metal, metal oxide and carbonaceous materials from inorganic–organic hybrid materials including various coordination polymers and gels [25–28]. Recently, we have developed an alternative strategy for the fabrication of symmetrical coralloid Cu 3D superstructures with surface interspersed with clusters of Cu nanoparticles by direct pyrolysis of the $[Cu_3(btc)_2]$ (btc = benzene-1,3,5-tricarboxylato) metal-organic framework (MOF) in a one-end closed horizontal tube furnace (OCTF) and realize the transformation from Cu(II)-carboxylate inorganic–organic hybrid coordination polymers to Cu nanostructures during the pyrolysis process [29].

Herein, we report a facile one-step synthesis of single-crystal Fe_3O_4 nanosheets (NSs) with average edge length in the range of 80–100 nm and thickness of about 30 nm via direct pyrolysis of EDTA ferric sodium salt in the OCTF system by controlling right pyrolysis temperature and reaction time. During our synthetic process, all the Fe transformed into Fe_3O_4 and no other iron oxide was detected. Based on Fe and Fe_3O_4, the yield of the reaction is 15.8% and 21.8%, respectively. Furthermore, the saturation magnetization of the Fe_3O_4 NSs is higher than the octahedral, wire, and hollow sphere structures [11–15]. Moreover, the possible formation mechanism of Fe_3O_4 NSs was also discussed.

2. Materials and methods

2.1. Synthesis of single-crystal Fe_3O_4 NSs

All of the reagents were of analytical grade and used as received without any further purification. Deionized water was used in the experiments. Ethylenediaminetetraacetic acid ferric sodium salt ($C_{10}H_{12}O_8N_2FeNa{\cdot}3H_2O$, 98%) and absolute ethanol (C_2H_5OH) were purchased from China National Medicines (Group) Shanghai Chemical Reagents Company. Thermal decomposition was carried out in a horizontal tube autofurnace and the synthetic process is illustrated in Scheme 1. In a typical synthesis, EDTA ferric sodium salt (1.0 g) was placed in a ceramic boat (with inside diameter of 0.6 cm and length of 5 cm) and then transferred into an horizontal quartz tube (with inside diameter of 3 cm and length of 40 cm) and calcined with one end of the tube closed in the horizontal tube furnace for 6 h with the heating rate of 10 °C/min at 350, 400, 500, and 550 °C, respectively. The final products were washed with deionized water and absolute ethanol for three times and dried in vacuum at 80 °C for 12 h.

2.2. Characterization

The powder X-ray diffraction (XRD) patterns were recorded on a Shimadzu XRD-6000 (operating at 40 kV and 30 mA) using Cu Ka radiation (wavelength λ = 1.5147 Å) in the 2θ range 20–80°. Fourier transform infrared spectra (IR) were obtained with Bruker Vectortm 22 FTIR spectrometer at a resolution of 4 cm^{-1} with a Nic-Plan IR microscope. Transmission electron microscopy (TEM) images were examined on JEOL JSM-2100 TEM using at an accelerating voltage of 200 kV. Magnetic properties were investigated using a vibrating sample magnetometer (VSM, Lake Shore 7303-9309 VSM). Thermal gravimetric analysis (TG) was studied on a PerKinElmer Pyris 1 TGA (USA).

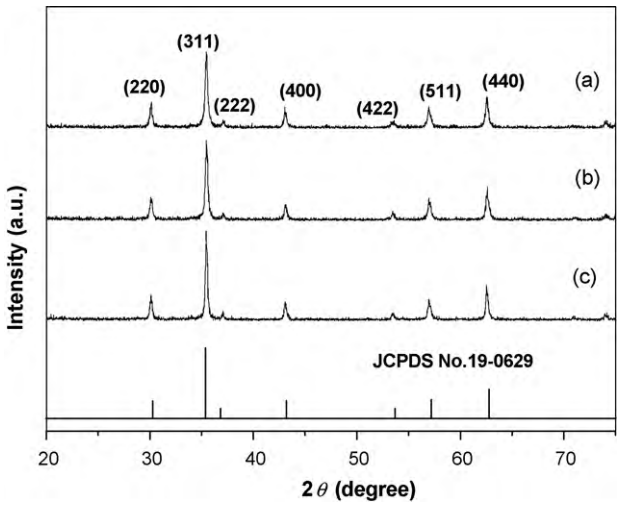

Fig. 1. XRD patterns of the synthesized products at (a) 350 °C, (b) 400 °C, and (c) 500 °C for the same reaction time of 6 h.

3. Results and discussion

The crystal structure and phase purity of the products was first characterized by XRD and FT-IR. Fig. 1 shows the XRD patterns of the synthesized products at (a) 350 °C, (b) 400 °C, and (c) 500 °C for the same reaction time of 6 h. All diffraction peaks can be indexed as inverse spinel structure Fe_3O_4, which is consistent with the standard value for bulk Fe_3O_4 phase (JCPDS file No. 19-0629). The broad peaks are ascribed to the nanocrystalline nature of the synthesized products prepared with the present approach. Furthermore, typical FT-IR spectra of the Fe_3O_4 products at (a) 350 °C, (b) 400 °C, and (c) 500 °C for the same reaction time of 6 h are presented in Fig. 2. The strong peaks at about 560 cm^{-1} are assigned to the vibration of the Fe–O bond of Fe_3O_4. The broad bonds at about 3500 and 1630 cm^{-1} are related to the absorbed H_2O molecules or OH^- on the surface of Fe_3O_4. These results indicate that the synthesized products are pure products without impurities.

The TEM images of Fe_3O_4 products at 350 °C for 6 h are shown in Fig. 3 to illuminate the morphology of the as-prepared products. As shown in Fig. 3a, large-scale Fe_3O_4 NSs were obtained. From higher resolution TEM images in Fig. 3b and c, Fe_3O_4 NSs with average edge length of 80 nm and thickness of about 30 nm can be seen. Furthermore, the high resolution TEM (HR-TEM) images (in

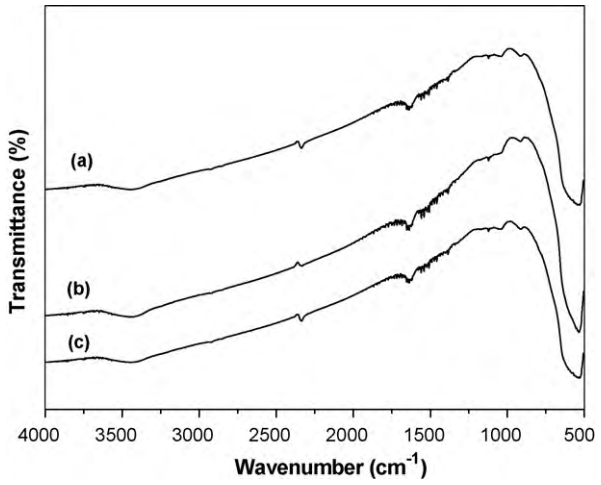

Fig. 2. FT-IR spectra of the synthesized products at (a) 350 °C, (b) 400 °C, and (c) 500 °C for the same reaction time of 6 h.

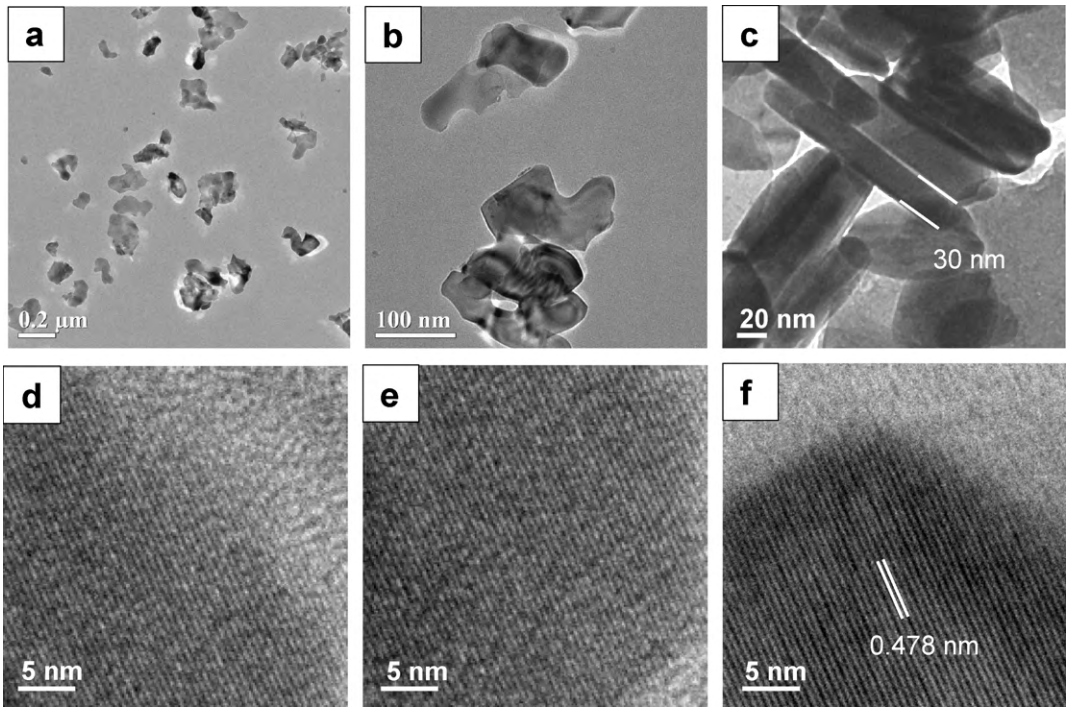

Fig. 3. (a–c) TEM and (d–f) HR-TEM images of the products at 350 °C for 6 h.

Fig. 3d–f) of different parts of the synthesized Fe_3O_4 NSs demonstrates that the formed Fe_3O_4 NSs show a single-crystal structure, and a lattice spacing of ca. 0.48 nm corresponds to the (1 1 1) planes of a spinel-structured iron oxide. Fig. 4 displays the particle size distribution of the products at 350 °C for 6 h. As can be seen, the synthesized Fe_3O_4 NSs display a narrow distribution mainly in the range of 70–90 nm, which is consistent with the TEM observation.

The morphology of the products is strongly affected by the pyrolysis temperature as shown in Fig. 5. By simple altering temperature from 400 to 600 °C for the same reaction time of 6 h, different products were obtained. At 400 °C for 6 h, sheet-like structured Fe_3O_4 with average edge length of 90 nm appeared (see Fig. 5a). With further increase of temperature to 500 °C, Fe_3O_4 NSs with average edge length of 100 nm (in Fig. 5b) were also obtained. When temperature increases to 600 °C, irregular structures (in Fig. 5c) appeared. Moreover, XRD patterns in Fig. 1 show that all the synthesized products at 400 and 500 °C were pure phase Fe_3O_4. Fig. 6 shows the XRD patterns of the products by pyrolysis of the EDTA ferric sodium salt at different temperatures for different reaction times, which indicates that all the samples were Fe_3O_4.

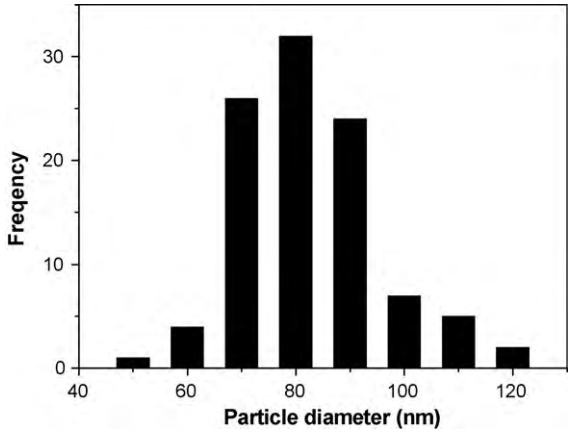

Fig. 4. The particle size distribution of the products at 350 °C for 6 h.

The magnetization in Fig. 7 shows the magnetization hysteresis loops of the Fe_3O_4 products. It can be seen that all of the products prepared at 350–400 and 500 °C for the same reaction time of 6 h are ferromagnetic at room temperature. The saturation magnetization

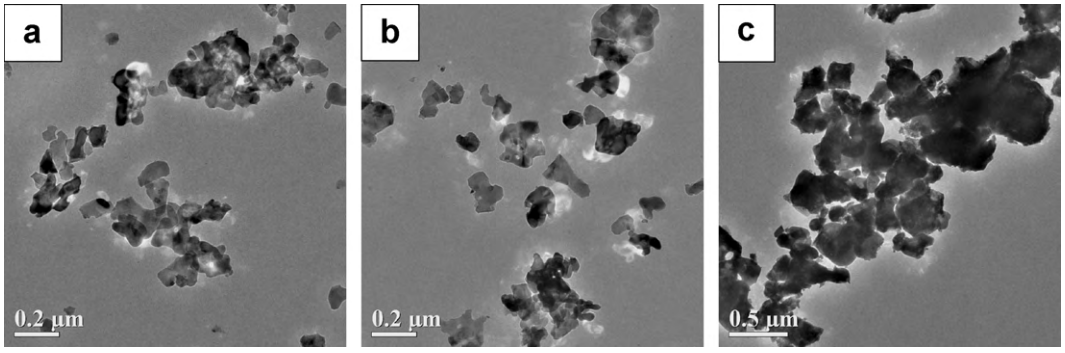

Fig. 5. TEM images of the products at (a) 400 °C, (b) 500 °C and (c) 550 °C for the same reaction time of 6 h.

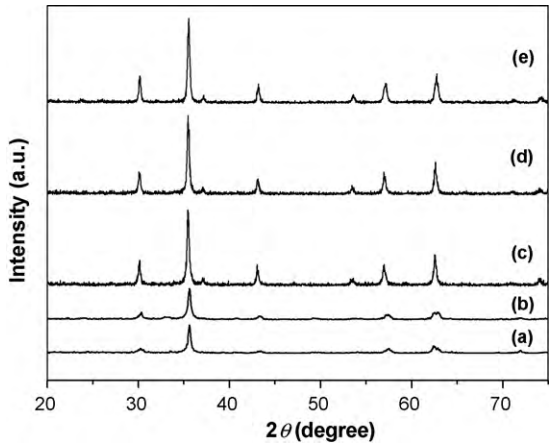

Fig. 6. XRD patterns of the synthesized products (a) at 200 °C for 6 h, (b) at 250 °C for 6 h, (c) at 300 °C for 6 h, (d) at 350 °C for 3 h, and (e) at 350 °C for 12 h.

(Ms) values of the Fe_3O_4 NSs decreasesed from 52.6 emu/g (350 °C) to 45.5 emu/g (400 °C) and 41.8 emu/g (500 °C), which is mainly due to particle size and crystallinity. Moreover, the coercive field (Hc) ascends from 180 to 230 and 250 Oe with the increased size of Fe_3O_4 NSs. The saturation magnetization is lower than that of bulk Fe_3O_4. In general, the magnetic properties of particles may be influenced by various factors including the size, structure, surface disordering, morphologies, etc. In our investigation, the reduced value might be due to the existence of non-magnetic carbon decomposed from EDTA on the surface and the spin canting of surface Fe atoms [30,31] as well as the strong effect of sheet orientation on the demagnetizing field [32–34] may result in the lower MAGNETIZATION and saturation magnetization of Fe_3O_4 NSs.

In general, carbon reductive method has been widely used for the synthesis of metal oxide nano- and microstrucures such as ZnO nanowires, nanobelts, nanosheets, and nanocastles and In_2O_3 octahedrons which use the mixture of metals (or metal oxides) and carbon as precursors [35–42]. Recently, Wang et al reported the controlled synthesis of Fe_3O_4 powder via carbothermal reduction method using pure Fe_2O_3 powder and glucose mixture as starting materials [43]. Carbon reductive method uses metals and metal oxides as precursors, which needs high reaction temperature above 500 °C of metal oxides and metals even beyond 1000 °C. However, our method needs lower temperature of the complete decomposed temperature of the EDTA ferric sodium salt. Fig. 8 shows the TGA–DTG curves of the EDTA ferric sodium salt in the air. There are three different weight-loss peaks at the temperature ranges of

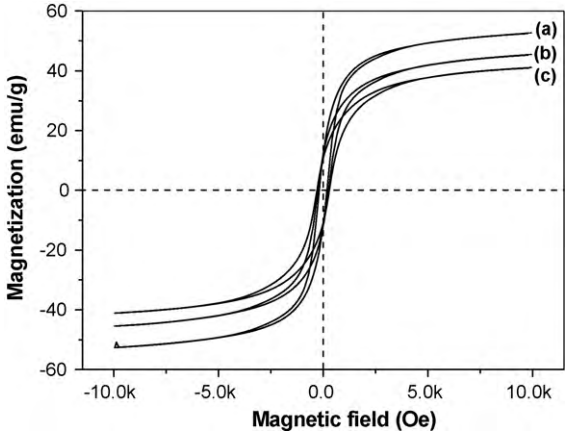

Fig. 7. Magnetic hysteresis loops at room temperature of the synthesized Fe_3O_4 NSs at (a) 350 °C, (b) 400 °C, and (c) 500 °C for the same reaction time of 6 h.

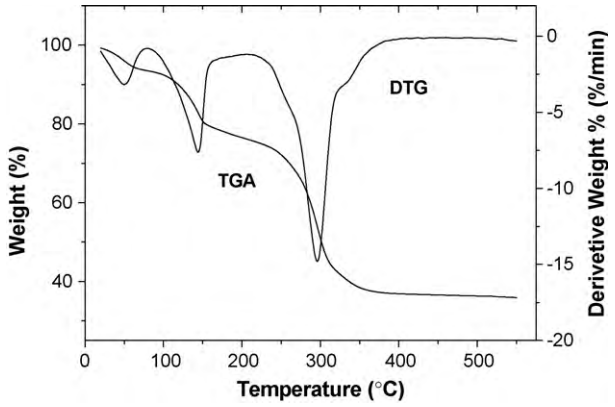

Fig. 8. TGA–DTG curves of the EDTA ferric sodium salt with the heating rate of 10 °C/min in a flowing air atmosphere.

25–120, 120–250, and 250–350 °C. The first weight-loss peak corresponds to the removal of adsorbed water. The second is mainly attributed to the desorption of crystal water in the EDTA ferric sodium salt. And the third one is ascribed to the decomposition of the EDTA ferric sodium salt to form iron oxides at high temperature. The coordination between carboxyl and ferric ions is an important factor for the formation of magnetite in the pyrolysis process. A possible formation mechanism of Fe_3O_4 NSs from the EDTA ferric sodium salt is discussed in the following. With the increase of thermal decomposition temperature, the EDTA ferric sodium salt began to lose its organic parts, which decomposed into carbon, and different gases including hydrogen and carbon monoxide, together with other fragments from the incomplete decomposed parts [25,44–48]. Reduction by the formed carbon and decomposed gases converted part of Fe^{3+} into Fe^{2+}. Finally, Fe_3O_4 was formed in the reductive atmosphere. Sodium carboxylate is a well-known protective agent for the synthesis of Fe_3O_4 and prominently affects the shape of the final products [49,50]. During the pyrolysis process, irregular Fe_3O_4 powders were formed and then NCs grow up with the increase of reaction time. When thermal decomposition was carried out in the air, the final product is Fe_2O_3, even when other experimental conditions are kept the same. The further formation mechanism of Fe_3O_4·NCs is still under investigation.

4. Conclusions

In summary, we have developed a novel and facile approach for controllable fabrication of single-crystal Fe_3O_4 NSs by direct pyrolysis of EDTA ferric sodium salt in the OCTF system in the air. The results indicate that the size and shape of the resultant products are sensitive to pyrolysis temperature and reaction time. By controlling the two parameters, single-crystal Fe_3O_4 NSs with edge length in the range of 80–100 nm and thickness of about 30 nm were successfully obtained. Moreover, a possible mechanism was also discussed. In prospect, this method is simple and facile and could synthesize other metal oxides under such experimental conditions.

Acknowledgment

This work was financially supported by the Scientific Research Foundation for Talent Introduction of Chongqing University (0903005104705) and the Students Research Training Program of Chongqing University.

References

[1] S. Laurent, D. Forge, M. Port, A. Roch, C. Robic, L. Vander Elst, R.N. Muller, Chem. Rev. 108 (2008) 2064–2110.

[2] K. Cheng, S. Peng, C.J. Xu, S.H. Sun, J. Am. Chem. Soc. 131 (2009) 10637–10644.
[3] B. Feng, R.Y. Hong, Y.J. Wu, G.H. Liu, L.H. Zhong, Y. Zheng, J.M. Ding, D.G. Wei, J. Alloys Compd. 473 (2009) 356–362.
[4] Z. Li, L. Wei, M.Y. Gao, H. Lei, Adv. Mater. 17 (2005) 1001–1005.
[5] S.M. El-Sheikh, F.A. Harraz, K.S. Abdel-Halim, J. Alloys Compd. 487 (2009) 716–723.
[6] S.H. Liu, R.M. Xing, F. Lu, R.K. Rana, J.J. Zhu, J. Phys. Chem. C 113 (2009) 21042–21047.
[7] L.Y. Chen, Z.X. Xu, H. Dai, S.T. Zhang, J. Alloys Compd. 497 (2010) 221–227.
[8] E.H. Kim, Y. Ahn, H.S. Lee, J. Alloys Compd. 434–435 (2007) 633–636.
[9] A.G. Yan, X.H. Liu, G.Z. Qiu, H.Y. Wu, R. Yi, N. Zhang, J. Xu, J. Alloys Compd. 458 (2008) 487–491.
[10] H. Deng, X.L. Li, Q. Peng, X. Wang, J.P. Chen, Y.D. Li, Angew. Chem. Int. Ed. 44 (2005) 2782–2785.
[11] S.W. Cao, Y.J. Zhu, M.Y. Ma, L. Li, L. Zhang, J. Phys. Chem. C 112 (2008) 1851–1856.
[12] L.L. Li, Y. Chu, Y. Liu, D. Wang, J. Alloys Compd. 472 (2009) 271–275.
[13] Y. Xiong, J. Ye, X.Y. Gu, Q.W. Chen, J. Phys. Chem. C 111 (2007) 6998–7003.
[14] W.D. Zhang, H.M. Xiao, L.P. Zhu, S.Y. Fu, J. Alloys Compd. 477 (2009) 736–738.
[15] F.Q. Hu, K.W. MacRenaris, E.A. Waters, E.A. Schultz-Sikma, A.L. Eckermann, T.J. Meade, Chem. Commun. 46 (2010) 73–75.
[16] Z.H. Yang, P.J. Cai, L.Y. Chen, Y.L. Gu, L. Shi, A.W. Zhao, Y.T. Qian, J. Alloys Compd. 420 (2006) 229–232.
[17] O. Carp, L. Patron, A. Reller, Mater. Chem. Phys. 101 (2007) 142–147.
[18] X.Y. Zeng, J.L. Yuan, L.D. Zhang, J. Phys. Chem. C 112 (2008) 3503–3508.
[19] F. Davar, M. Salavati-Niasari, Z. Fereshteh, J. Alloys Compd. 496 (2010) 638–643.
[20] H. Thakuria, B.M. Borah, G. Das, Eur. J. Inorg. Chem. (2007) 524–529.
[21] K.E. Neo, Y.Y. Ong, H.V. Huynh, T.S. Andy Hor, J. Mater. Chem. 17 (2007) 1002–1006.
[22] M.C. Wu, C.S. Lee, Inorg. Chem. 45 (2006) 9634–9636.
[23] G. Marinescu, L. Patron, O. Carp, L. Diamandescu, N. Stanica, A. Meghea, M. Brezeanu, J.C. Greniere, J. Etourneau, J. Mater. Chem. 12 (2002) 3458–3462.
[24] L.Y. Chen, H. Xing, Y.M. Shen, J.F. Bai, G.Q. Jiang, J. Solid State Chem. 182 (2009) 1387–1395.
[25] L.Y. Chen, J.F. Bai, C.Z. Wang, Y. Pan, X.Z. You, Chem. Commun. (2008) 1581–1583.
[26] L.Y. Chen, H. Dai, Y.M. Shen, J.F. Bai, J. Alloys Compd. 491 (2010) L33–L38.
[27] L.Y. Chen, Y.M. Shen, J.F. Bai, Mater. Lett. 63 (2009) 1099–1101.
[28] L.Y. Chen, C.L. Zhao, J.F. Bai, Chem. Lett. 38 (2009) 276–277.
[29] L.Y. Chen, Y.M. Shen, J.F. Bai, C.Z. Wang, J. Solid State Chem. 182 (2009) 2298–2306.
[30] K. Woo, J. Hong, S. Choi, H. Lee, J. Ahn, C. Kim, S. Lee, Chem. Mater. 16 (2004) 2814–2818.
[31] J. Lu, X.L. Jiao, D.R. Chen, W. Li, J. Phys. Chem. C 113 (2009) 4012–4017.
[32] D. Jiles, Introduction to Magnetism and Magnetic Materials, Chapman & Hall/CRC, Taylor & Francis Group, Boca Raton, USA, 1998.
[33] R.C. O'Handley, Modern Magnetic Materials Principles and Applications, Wiley-Interscience, USA, 2000.
[34] A. Gómez-Ramírez, M.T. López-López, J.D.G. Durán, F. González-Caballero, Soft Mater. 5 (2009) 3888–3895.
[35] M.H. Huang, Y. Wu, H. Feick, N. Tran, E. Weber, P.D. Yang, Adv. Mater. 13 (2001) 113–116.
[36] Y. Ding, P.X. Gao, Z.L. Wang, J. Am. Chem. Soc. 126 (2004) 2066–2072.
[37] J.H. Park, H.J. Choi, Y.J. Choi, S.H. Sohn, J.G. Park, J. Mater. Chem. 14 (2004) 428–435.
[38] S.Q. Xi, X.K. Liu, P.L. Li, J.G. Zhou, J. Alloys Compd. 457 (2008) 452–456.
[39] X. Wang, J. Song, Z.L. Wang, Chem. Phys. Lett. 424 (2006) 86–90.
[40] Z. Huang, C. Chai, X. Tan, J. Wu, A. Yuan, Z. Zhou, S. Liu, Chin. J. Inorg. Chem. 23 (2007) 499–503.
[41] Z.W. Yao, J. Alloys Compd. 475 (2009) L38–L41.
[42] S.P. Pang, F.F. Jian, L. Wang, Inorg. Chem. 47 (2008) 344–348.
[43] H. Wang, P. Hu, D. Pan, J. Tian, S. Zhang, A. Volinsky, J. Alloys Compd. 502 (2010) 338–340.
[44] Y. Li, J.P. Zhao, B. Wang, Mater. Res. Bull. 39 (2004) 365–374.
[45] R. Ran, Y.M. Guo, Y. Zheng, K. Wang, Z.P. Shao, J. Alloys Compd. 491 (2010) 271–277.
[46] X.F. Ding, Y.J. Liu, L. Gao, L.C. Guo, J. Alloys Compd. 458 (2008) 346–350.
[47] K. Guo, H.H. Chen, X.X. Guo, X.X. Yang, F.F. Xu, J.T. Zhao, J. Alloys Compd. 500 (2010) 34–38.
[48] A. Feldhoff, M. Arnold, J. Martynczuk, Th.M. Gesing, H. Wang, Solid State Sci. 10 (2008) 689–701.
[49] A.G. Yan, X.H. Liu, G.Z. Qiu, H.Y. Wu, R. Yi, N. Zhang, J. Alloys Compd. 458 (2008) 487–491.
[50] H.F. Zhou, R. Yi, J.H. Li, Y. Su, X.H. Liu, Solid State Sci. 12 (2010) 99–104.